Colloids and Surfaces B: Biointerfaces 122 (2014) 332–340

Contents lists available at ScienceDirect

Colloids and Surfaces B: Biointerfaces

journal homepage: www.elsevier.com/locate/colsurfb

# Cyclic RGD-modified chitosan/graphene oxide polymers for drug delivery and cellular imaging

Chen Wang[a,b], Binbin Chen[c], Meijuan Zou[a], Gang Cheng[a,*]

[a] Department of Pharmaceutics, School of Pharmacy, Shenyang Pharmaceutical University, Shenyang 110016, PR China
[b] School of Pharmacy, Xiamen Medical College, Xiamen 361008, PR China
[c] Department of Pharmacy, Xiamen Xianyue Hospital, 361012, PR China

ARTICLE INFO

*Article history:*
Received 31 March 2014
Received in revised form 11 July 2014
Accepted 13 July 2014
Available online 19 July 2014

*Keywords:*
Cyclic RGD
Graphene oxide
pH-responsive
Controlled release
Hepatoma cells targeting

ABSTRACT

Polymers based on cyclic RGD-modified chitosan/graphene oxide are investigated in this paper as an innovative type of drug delivery system for hepatocellular carcinoma-targeted therapy and imaging. The system was prepared using a simple noncovalent method by coating drug-loaded graphene oxide (GO) with cyclic RGD-modified chitosan (RC). The results show that an efficient loading of doxorubicin (DOX) on GO (1.00 mg/mg) was obtained. The system exhibits a pH-responsive behavior because of the hydrogen bonding interaction between GO and RC, and may be very stable under physiological conditions but with release at a lower pH (tumor environment). In addition, cellular uptake and proliferation studies using hepatoma cells (Bel-7402, SMMC-7721, HepG2) indicated that the cRGD-modified chitosan/graphene oxide polymer could recognize hepatoma cells and promote drug uptake by the cells, especially for cells overexpressing integrins. Together, these results demonstrate that the RC/GO polymers provide a multifunctional drug delivery system with the ability to target hepatocarcinoma cells, and are pH-responsive and can be efficiently loaded with a number of therapeutic agents for biomedical applications.



## 1. Introduction

Hepatocellular carcinoma (HCC) is one of the leading causes of cancer death worldwide. Mortality from liver cancer increased significantly from 1990 to 2005 by as much as 50%. Studies have reported an increase in hepatocellular carcinoma incidence in western countries, with a subsequent impact on liver cancer mortality [1]. Current chemotherapy for hepatocellular carcinoma is very limited owing to the toxicity of the drugs used to treat the disease in normal tissues and cells. To overcome this, the design of nanoscale drug delivery systems which optimize the selectivity of drugs and reduce toxic side effects is attracting great attention. New drug delivery systems (DDS) have been developed in recent years to target the liver, such as nanoparticles [2,3], polymer–drug conjugates [4], and carbon nanotubes [5]. The ideal drug delivery system, however, should exhibit several properties for successful cancer therapy including: targeted delivery [6–9], efficient loading [10] and controlled release [11,12].

Graphene [13], a two dimensional monoatomic thick building block of a carbon allotrope [14,15], is an ideal nanomaterial for drug delivery systems. As a potential nanocarrier, graphene oxide (GO) has attracted considerable attention because of its excellent biocompatibility [16–20] and well-dispersed stability in aqueous solution [21–24]. GO also has a large specific surface area and a large π-conjugated structure. Drugs, such as 5-fluorouracil, ibuprofen, camptothecin and doxorubicin [25–28], can be loaded onto GO via π–π stacking and van der Waals interaction. In addition, there are abundant epoxide, hydroxyl and carboxyl functional groups on GO, which can form strong hydrogen bond with a number of drugs. Chitosan (CS) has been widely reported to be a suitable biopolymer for drug delivery because of its excellent biocompatibility, biodegradability, and positive characteristics [29,30].

For successful active targeting, several specific ligands have been used for chitosan-based drug delivery systems through chemical modification, such as small molecules [31], antibodies [32], and peptides [33]. Among these ligands, integrin-mediated cyclic RGD peptides appear attractive candidates. This ligand exhibits a high binding affinity and selectivity for $\alpha_v\beta_3$ and $\alpha_v\beta_5$ integrin receptors, which are overexpressed in tumor vessels and most tumor cells [34–36]. RGD-modified polymers have therefore been exploited as an active targeting system for anticancer drug delivery

* Corresponding author. Tel.: +86 24 23986326; fax: +86 24 23986326.
*E-mail address:* chenggang63@hotmail.com (G. Cheng).

http://dx.doi.org/10.1016/j.colsurfb.2014.07.018
0927-7765/

[37–39]. The surface of HCC cells contains an abundance of specific integrin receptors, such as $\alpha_v\beta_3$ and $\alpha_v\beta_5$, although these receptors are rarely expressed in normal hepatocytes [40]. Until now, however, the graphene oxide mediated and c(RGDfK)-modified active targeting function of this drug delivery system has never been applied to HCC-targeted therapy and imaging.

In this paper, we describe how we explored and prepared an innovative multifunctional drug delivery system with properties of active targeting (hepatocarcinoma cell targeting), and pH-responsive and efficient loading, based on a c(RGDfK)-modified chitosan/graphene oxide polymer. In our strategy, the c(RGDfK) peptide and chitosan were conjugated by a thiolation reaction using a cross-linking reagent, N-succinimidyl 3-(2-pyridyldithio)-propionate (SPDP), to improve the specificity of cell targeting by polymers. The c(RGDfK)-modified chitosan (RC) was then analyzed and characterized by 1H nuclear magnetic resonance ($^1$H NMR) spectroscopy. Drug molecules, such as DOX, were noncovalently loaded onto GO via $\pi$–$\pi$ stacking interactions which were confirmed by spectroscopy. The amount of DOX loaded onto GO was very high and pH-dependent. The drug loading, release mechanisms and in vitro drug controlled release behavior were investigated and analyzed. Positive charges on RC appear to produce a strong noncovalent functionalization with a negatively charged GO surface, resulting in extensive coating of GO with RC, and it is expected that the positively charged RC may strongly adsorb negatively charged GO and significantly change the liver-targeting properties of its surface. The morphology of the polymers was studied using images obtained by atomic force microscopy (AFM). The cellular uptake studies were performed using a laser confocal fluorescence microscope (LCFM) and a high-content screening (HCS), while a cell proliferation test was carried out using a Cell Counting Kit-8 (CCK-8) cytotoxicity assay. The preparation and use of multifunctional DDS opens up new possibilities for the treatment of HCC.

## 2. Materials and methods

### 2.1. Materials

Human hepatoma cell lines (Bel-7402, SMMC-7721, HepG2) were obtained from the Key Laboratory of Xiamen Medical College (Xiamen, China). Cell lines were grown in high glucose Dulbecco's modified Eagle's Media (DMEM) containing 10% fetal bovine serum (FBS) and 100 U/mL penicillin G-streptomycin in a humidified incubator (5% $CO_2$) at 37 °C.

Cyclic RGD (c[RGDfK (Mpa)], MW691.84 Da) was purchased from ChinaPeptides Co., Ltd (Shanghai, China); graphene oxide was purchased from Nanjing XFNANO Materials Tech Co., Ltd (Nanjing, China); chitosan (deacetylation degree of 90% and MW of 50 kDa) was purchased from Shandong Qingdao Haidebei Biological Product Factory (Qingdao, China); N-succinimidyl 3-(2-pyridyldithio)-propionate (SPDP) was purchased from Sangon Biotech Co., Ltd (Shanghai, China); CCK-8 was purchased from Dojindo Molecular Technologies, Inc. (Kumamoto, Japan); fluorescein isothiocyanate (FITC) was purchased from Sigma–Aldrich (St. Louis, USA); and doxorubicin was purchased from Dalian Meilun Biological Product Factory (Dalian, China). All other reagents and solvents were of analytical grade.

### 2.2. Synthesis of cRGD-modified chitosan (RC)

The cRGD and CS were conjugated by a thiolation reaction using a cross-linking reagent, N-succinimidyl 3-(2-pyridyldithio)-propionate (SPDP). Briefly, the $NH_2$ group of CS (80 mg) was activated by the SPDP (3.2 mg) dissolved in 100 mL of HCl (0.1 M) buffer solution to react for 24 h at ambient temperature. Then, cRGD (7.2 mg) was added to SPDP-activated CS solution and stirred for 24 h at room temperature. The resulting cRGD-modified chitosan was purified using a dialysis tube (MWCO = 3500) and dialyzed for three days against distilled water and then freeze-dried (Christ Alpha2-4 LSC, Germany) to obtain cRGD-modified chitosan. The composition of the cRGD group in cRGD-modified chitosan was confirmed by $^1$H NMR spectroscopy (Bruker Advance 400 MHz, Germany).

FITC-labeled RC was synthesized according to a previously published procedure [41] with minor modification. RC (1.0 g) was dissolved in 100 mL of 0.1 M acetic acid, followed by the addition of dehydrated methanol (100 mL) and FITC (2 mg/mL in methanol, 50 mL). The reaction was run for 3 h in the dark at room temperature. The FITC-labeled RC (FITC/RC) was then precipitated by rising the pH to 9.5 with 0.5 M NaOH. The resulting precipitate was washed with deionized distilled water and separated by centrifuge until there was complete absence of fluorescence signal in the supernatant. The FITC-labeled RC was then dissolved in 0.1 N acetic acid and dialyzed in deionized distilled water for three days. Finally, the FITC-labeled RC was obtained by lyophilization.

### 2.3. Loading of GO with DOX (GO–DOX) and its characterization

The GO aqueous suspension was subjected to sonication (Sonics VCX750, USA) for 30 min to obtain a homogenous solution. DOX loading onto GO was carried out by mixing DOX (30 mg) with GO (20 mg) in 100 mL phosphate buffered saline solution (pH 7.4) and stirred for 24 h at ambient temperature in darkness. The product was then centrifuged (Sigma 3-30K, Germany) at 18,000 rpm for 30 min and washed three times until the supernatant became colorless [42,43]. GO–DOX was obtained by lyophilizing the aqueous solution and stored at 4 °C. The resultant GO–DOX product was characterized by UV–vis spectrophotometry (Shimadzu V-1800, Japan), and FT-IR spectrometry (Perkin Elmer spectrum 100, USA). The drug loading ability of GO was studied by Ultra Performance Liquid Chromatography (Waters ACQUITY UPLC, USA). The drug loading ability was calculated according to experimental equation:

$$\text{Drug loading ability}\ \ (\text{mg/mg}) = \frac{W_{\text{added}} - W_{\text{free}}}{W_{\text{GO}}} \quad (1)$$

where $W_{\text{added}}$ denotes the weight of initial DOX added, $W_{\text{free}}$ is the weight of DOX in centrifuged solution, and $W_{\text{GO}}$ is the weight of GO used in formulations.

The estimated drug loading ability was $1.00 \pm 0.05$ mg/mg ($n = 3$).

### 2.4. Fabrication and characterization of RC–GO–DOX polymers

To prepare RC–GO–DOX polymers, GO–DOX (20 mg) was mixed with RC (40 mg) in 100 mL phosphate buffered saline solution (pH 7.4). The mixture was then stirred overnight at ambient temperature and protected from bright light. Free DOX and RC were completely removed by centrifugation (18,000 rpm, 30 min) and washed three times with PBS solution until the supernatant was colorless, followed by lyophilization. The drug loading efficiency (%) was calculated by the following formula:

$$\text{Drug loading efficiency}\ \ (\%) = \frac{W_{\text{loaded}} - W_{\text{free}}}{W_p} \times 100 \quad (2)$$

where $W_{\text{loaded}}$ is the weight of DOX loaded on GO, $W_{\text{free}}$ is the weight of DOX in the supernatant after reaction, and $W_{\text{p}}$ is the weight of polymers (RC–GO–DOX).

The drug loading efficiency was 87%.

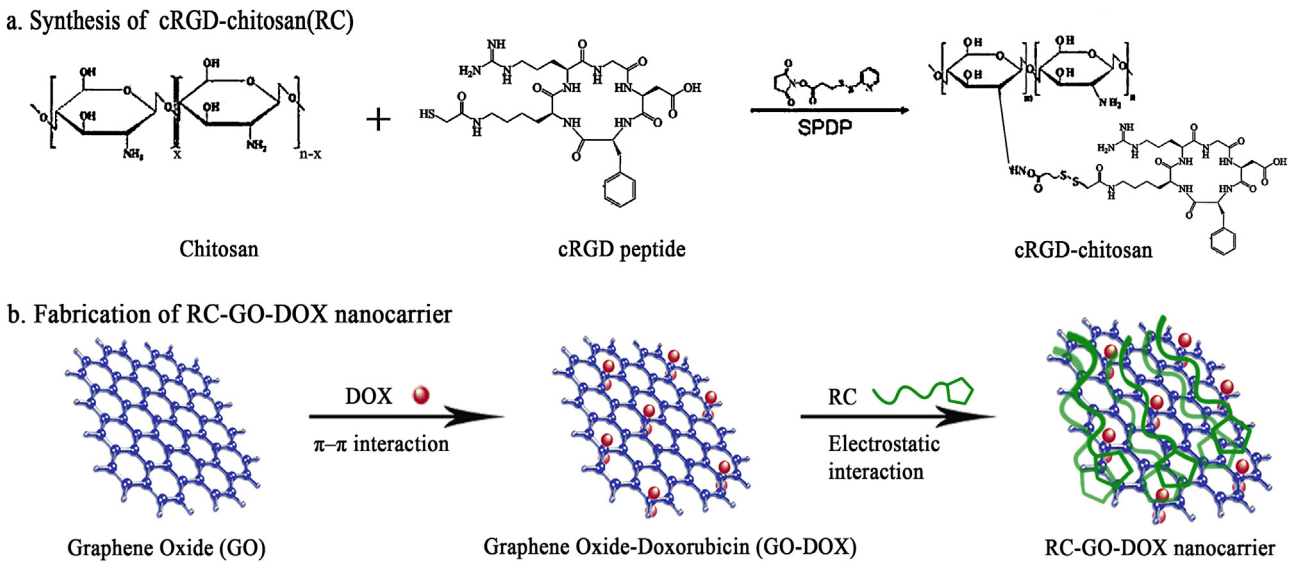


**Fig. 1.** Schematic representation of the synthesis of cRGD-modified chitosan and preparation of nanocarrier RC–GO–DOX. Top: scheme-(a); bottom: scheme-(b).

### 2.5. In vitro drug release assay

The dynamic dialysis method was used to examine the drug release of GO–DOX and RC–GO–DOX. GO–DOX and RC–GO–DOX samples were dialyzed using dialysis membrane bags (3500 MW cutoff) in 50 mL PBS buffered solution at 37 °C. The dialysis process was performed at pH 5.5 (cancer cell environment) and 7.4 (normal physiological conditions). As soon as the dialysis bags were placed into the reservoir, the drug release was determined. At various time intervals, aliquots (2.5 mL) were withdrawn and replaced with a fresh dissolution medium. The concentration of DOX released from the samples into PBS buffer solution was analyzed with by UPLC as described above in Section 2.3.

### 2.6. Cellular uptake study of the polymer

HepG2 cells, SMMC-7721 cells and Bel-7402 cells were used in this study. For the confocal microscope study, HepG2 cells, SMMC-7721 cells and Bel-7402 cells were cultured in the 35 mm glass bottom dishes (NEST). The cells were incubated with FITC/RC–GO and FITC/CS–GO polymer solution at the same concentration for 2 h. The polymer solution was then removed and the cells were washed three times with 1 mL PBS. The cellular localization was then observed by LCFM (Olympus FV1000, Japan).

For quantitative analysis of cellular uptake, HepG2 cells, SMMC-7721 cells and Bel-7402 cells were planted in 96-well plates at a density of $5 \times 10^3$ cells per well and incubated for 24 h at 37 °C in a 5% $CO_2$ atmosphere, respectively. FITC/RC–GO and FITC/CS–GO polymer solution were then added to the culture. After incubating at 37 °C for 2 h, the medium of wells was removed and the wells were washed with PBS three times. The assay plates were then initially imaged and analyzed using the Cell Health Profiling BioApplication on an ArrayScan® XTI High Content Analysis Reader (Thermo Fisher Scientific Cellomics, USA) using a 20× objective.

### 2.7. Cell proliferation assay

The cell proliferation tests of the polymers without loading anti-cancer drug (FITC/RC–GO), drug-loaded CS/GO polymers (FITC/CS–GO–DOX), drug-loaded RC/GO polymers (FITC/RC–GO–DOX), and free drug (DOX) were determined from their cytotoxicity on three hepatoma cell lines (HepG2 cells, SMMC-7721 cells and Bel-7402 cells) using a CCK-8 assay. Six concentrations of each sample were applied to target the cancer cells. For the CCK-8 assays, three hepatoma cell lines were plated into 96-well microtiter plates at a density of $5 \times 10^3$ cells in growth medium. After a 48 h incubation with FITC/RC–GO, FITC/CS–GO–DOX and FITC/RC–GO–DOX, the number of viable cells was counted using CCK-8 according to the manufacturer's instructions. The absorbance of each sample was measured using an ELISA reader (Tecan Infinite M1000 PRO, Switzerland), at a test wavelength of 450 nm and a reference wavelength of 600 nm. Inhibition of proliferation was calculated based on a percentage of control wells containing cell culture medium without the drug.

## 3. Results and discussion

### 3.1. Synthesis and characterization of cRGD-modified chitosan conjugate

The synthesis of cRGD-modified chitosan is illustrated in Fig. 1a. The synthesis of cRGD-modified chitosan is confirmed by the $^1$H NMR. As shown in Fig. 2, peaks for the $CH_2$ of methylene in RGD

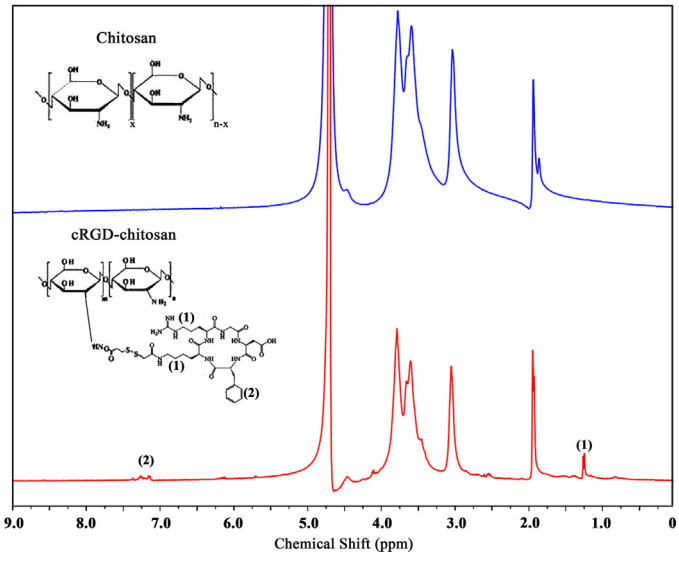


**Fig. 2.** $^1$H NMR spectrum of cRGD-modified chitosan.

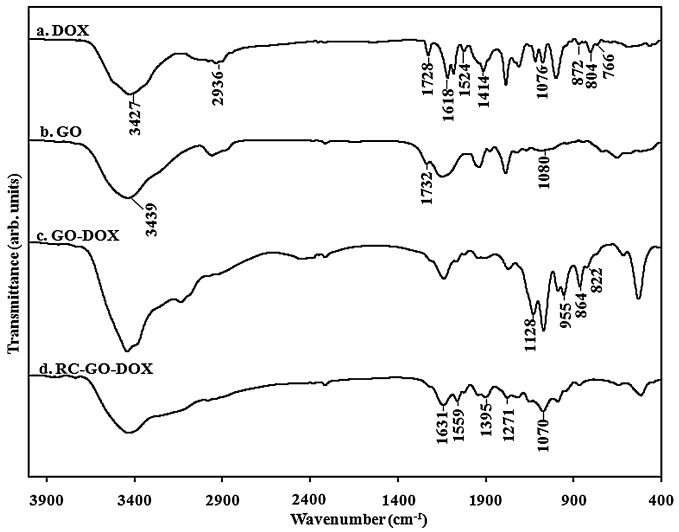


**Fig. 3.** FT-IR spectra of (a) DOX, (b) GO, (c) GO–DOX, and (d) RC–GO–DOX.

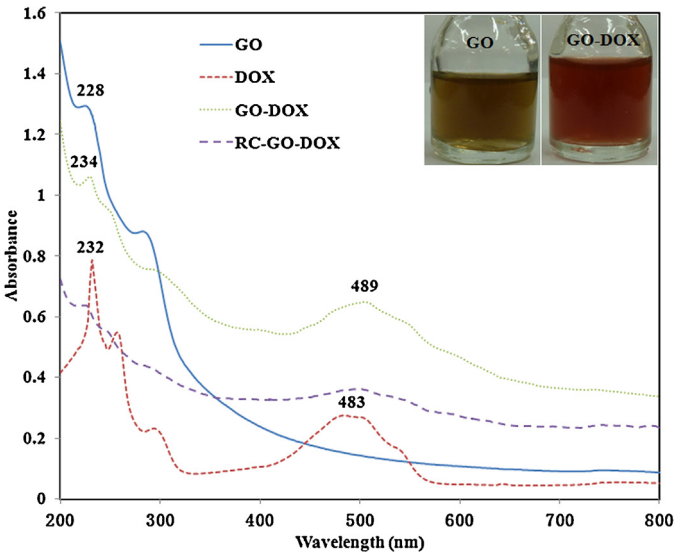


**Fig. 4.** UV analysis of DOX, GO, DOX–GO and RC–DOX–GO measured at 483 nm by UV–vis spectrophotometry. Inset: the color of GO and GO–DOX in aqueous solution is shown.

(1) and the CH of the benzene group in RGD (2) were observed at $\delta$ = 1–2 ppm and 7–8 ppm, respectively. This result is consistent with previous findings [44].

### 3.2. Drug loading mechanisms and their characterization

For successful anticancer drug delivery, the drug carriers have to be constructed to respond to a specific stimulus, and to achieve a high drug loading capacity. Compared with pristine graphite, GO is heavily oxygenated carrying hydroxyl and epoxy groups on the $sp^3$ hybridized carbon on the basal plane, in addition to carbonyl and carboxyl groups located at the sheet edges on the $sp^2$ hybridized carbon [45]. The interaction between GO and DOX may come from π–π staking between the conjugated structure of the graphene sheet and the quinone portion of DOX and the hydrophobic effect between. Also, hydrogen bonding between the —OH, —COOH groups of GO and the —OH, —$NH_2$ groups of DOX may take place. The FT-IR and UV–vis spectra confirm that DOX is successfully loaded onto GO, and the loading capacity of GO was studied by UV–vis spectroscopy.

In the FT-IR spectrum (Fig. 3a), DOX exhibits characteristic absorption peaks of quinone and ketone carbonyl groups at 3427, 2936, 1728, 1618, 1414 and 1076 $cm^{-1}$. N—H stretching bands (1524 $cm^{-1}$) and C—O—$CH_3$ stretching bands (804 $cm^{-1}$) were observed. The peaks at 872 and 766 $cm^{-1}$ were assigned to the primary amine wagging and N—H deformation bonds respectively.

Fig. 3b shows the FT-IR spectrum of GO. The spectrum of GO confirmed the presence of OH (3439 $cm^{-1}$) and C=O (1732 $cm^{-1}$), and the peak at 1080 $cm^{-1}$ is characteristic of the C—O—C stretching vibration, and confirms the presence of GO. After formation of GO–DOX polymers, several new peaks were found in addition to the

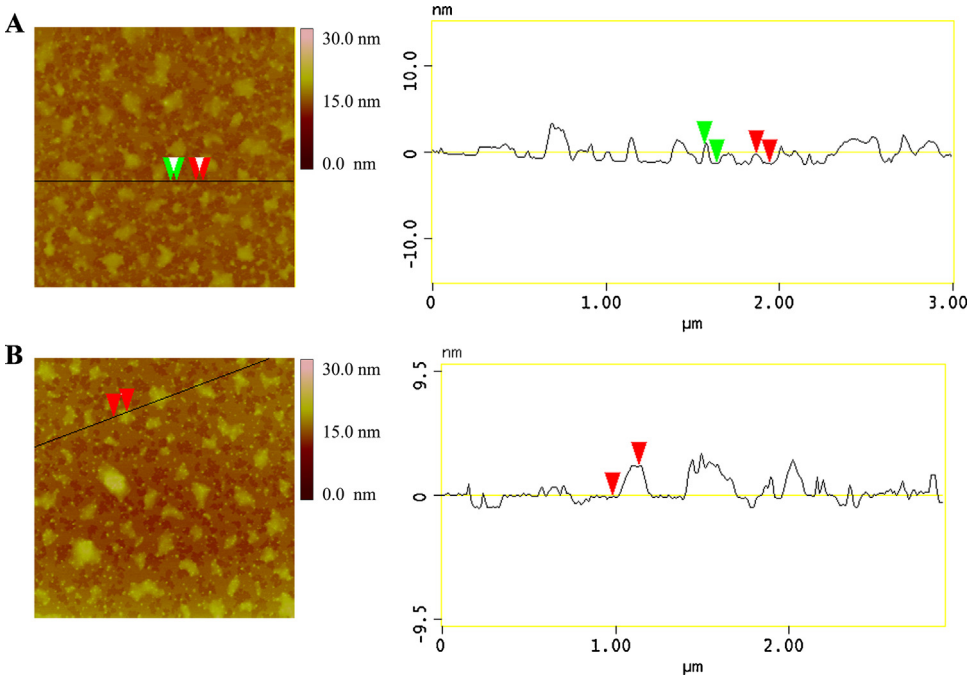


**Fig. 5.** AFM observation (A) GO and (B) RC–GO–DOX.

original peaks from GO itself, as shown in Fig. 3c. The new absorption peaks at ~1128 and 822 $cm^{-1}$ were assigned to the stretching bands of C—O—$CH_3$ of DOX, and the peaks at ~955 and 864 $cm^{-1}$ were attributed to the primary amine wagging and N—H deformation bonds of DOX, respectively. The observation of new peaks may be due to non-covalent interactions (mainly hydrogen bonding) between GO and DOX [46]. These changes confirm that DOX was successfully loaded on GO, and the color of the GO aqueous solution changed from brown to dark red after loading with DOX, as shown in the inset in Fig. 4.

More convincing evidence of the interaction between GO and DOX is provided by UV–vis spectroscopy (Fig. 4). It was observed that four separate characteristic absorption peaks of DOX were located at 232, 255, 291 and 483 nm, and GO showed a single broad peak at 228 nm. After forming the polymers, the peaks of DOX show a bathochromic shift: for example, after hybridization with GO, the absorption peaks of DOX at 232 and 483 nm shifted to 234 and 489 nm, respectively. It is generally believed that the interaction of a ground-state electron donor–acceptor between the two compounds led to the red-shift [47,48].

### 3.3. Polymers of RC–GO–DOX

There are a number of negatively charged functional groups (carboxyl, hydroxyl, and epoxide) on the GO surface in aqueous solution, which may interact with positively charged polymers [49,50]. Consequently, GO can be coated with RC using a non-covalent method in order to retain the intrinsic pH-responsive properties of GO and RC. The production process of RC–GO–DOX polymers is shown in Fig. 1b.

Fig. 3d shows the FT-IR spectra of the GO–DOX coating with RC (RC–GO–DOX). The broad peak between 3600 and 3000 $cm^{-1}$ was assigned to the amine stretching from the cRGD-modified chitosan and the —OH groups from graphene oxide. Compared with pristine graphene oxide, the peak at 1631 $cm^{-1}$ was attributed to the C=C groups from GO and showed a downshift. A broad peak at 1070 $cm^{-1}$ was due to C—O—C stretching from the GO layers [51]. All of the above results confirm that an interaction took place between RC and GO.

The morphology and thickness of RC–GO–DOX and GO were characterized by AFM (Veeco MultiMode Nanoscope IIIa controller, USA). RC–GO–DOX showed the average thickness of 2.3 nm which was significantly greater than that of GO (~1.1 nm), as shown in Fig. 5. This result could be due to the RC being grafted onto both sides of GO through a hydrophobic interaction and the van der Waals force between RC and GO, similar to other polymers that interact with GO as reported previously [52,53]. Zeta potential measurements were performed on a Malvern Zetasizer Nano-ZS90 particle analyzer. As shown in Table S1, GO exhibited the zeta potential of −33.6 mV while the zeta potential of RC–GO–DOX reversed to 31.6 mV, also suggesting the complexation of RC with GO.

Supplementary Table S1 related to this article can be found, in the online version, at http://dx.doi.org/10.1016/j.colsurfb.2014.07.018.

### 3.4. Drug release behavior

The comparative release profiles of DOX from GO–DOX and RC–GO–DOX in two different release buffers (PBS, pH 5.5 and 7.4) are shown in Fig. 6a. It was observed that the release profile of DOX from GO–DOX and RC–GO–DOX was pH-responsive. The drug release from the polymer, which may have excellent stability under normal physiological conditions but with release at a lower pH (cancerous tissue environment), is important in clinical situations for selective drug release [54]. With the same materials, it is found

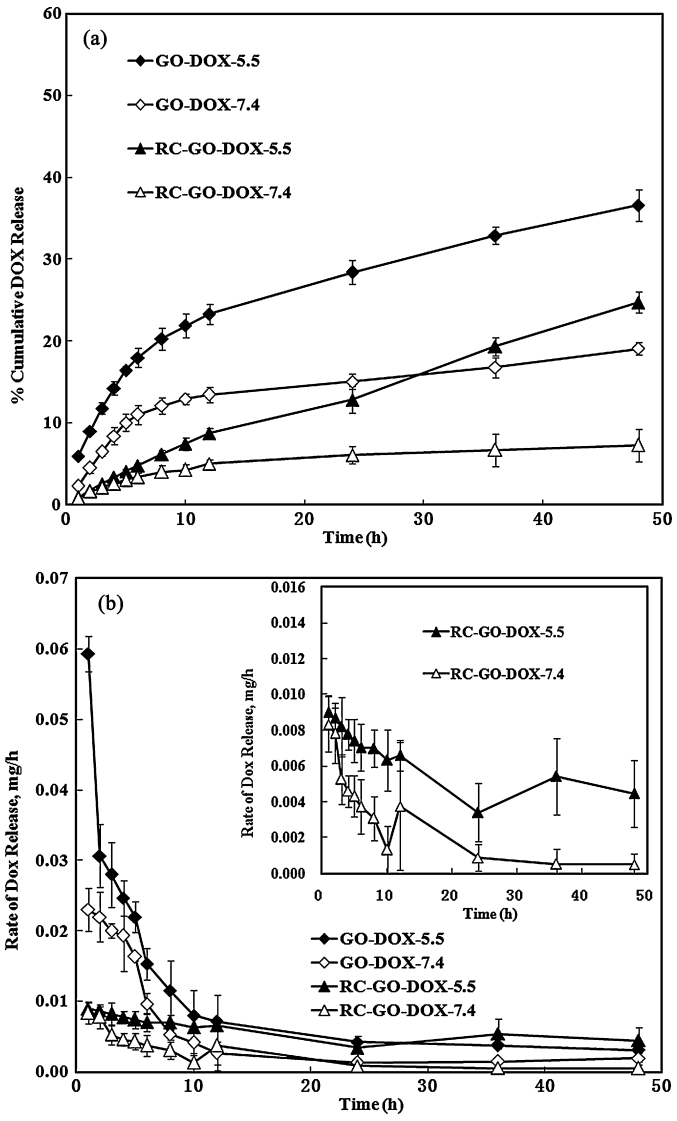


**Fig. 6.** (a) In vitro release profile of GO–DOX and RC–GO–DOX in phosphate buffer solution (pH 5.5 and 7.4) at 37 °C. (b) Rate of DOX release from GO–DOX and RC–GO–DOX in phosphate buffer solution (pH 5.5 and 7.4) at 37 °C. The values given are mean ± SD and $n = 3$.

that the amount of DOX released from the polymer at pH 5.5 was much greater than that released at pH 7.4. For the time points after 48 h, 36.6% of DOX was released from GO–DOX at pH 5.5, while only 19.1% of DOX was released at pH 7.4. This trend is attributed to the hydrogen-bonding interaction between DOX and GO. This interaction is stronger under neutral conditions (pH 7.4), and results in an inefficient release. At the same pH, the release behavior of RC–GO–DOX indicates that 7.3% of DOX was released from RC–GO–DOX after 48 h at pH 7.4, which is much lower than that from GO–DOX. This may be explained by the fact that when the drug passes through the macromolecular networks, the coated film of biodegradable cRGD-modified chitosan offers an additional barrier. Apart from the diffusion effect, the release of DOX is also caused by the degradation of the cRGD-modified chitosan film.

Fig. 6b shows the release rate of DOX from drug-loaded polymers. Clearly, the profile shows a slow release rate of RC–GO–DOX in the first 10 h (pH 5.5 or pH 7.4), since coating with RC films reduces the drug release rate. Such results may be due to the degradation of RC films, as indicated in the above section.

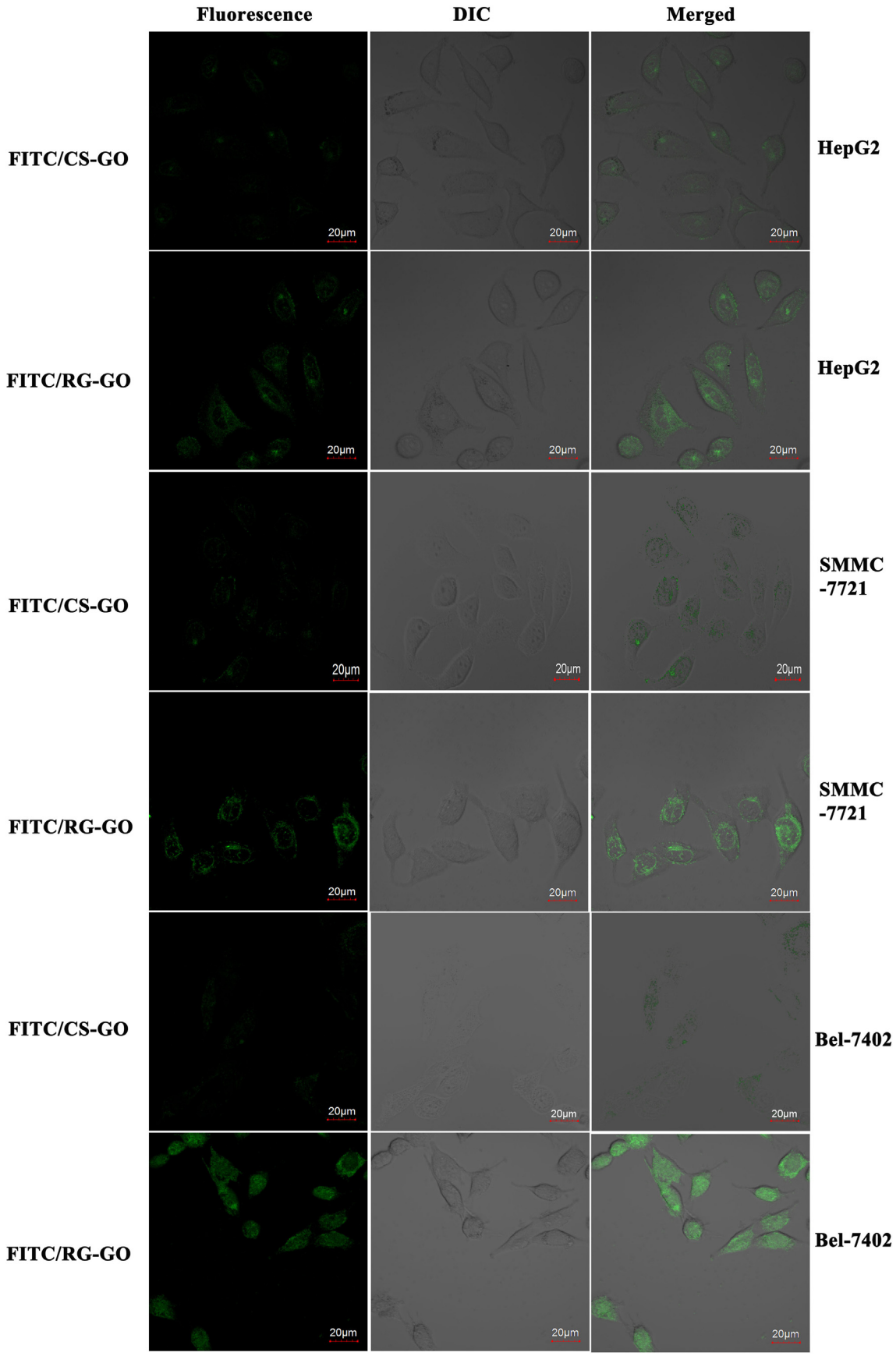


**Fig. 7.** The cell targeting ability of FITC/RC–GO and FITC/CS–GO in different hepatoma cells lines. Intracellular uptake of FITC/RC–GO and FITC/CS–GO in HepG2 cells, SMMC-7721 cells and Bel-7402 cells respectively after incubation for 2 h; scale bar = 20 μm.

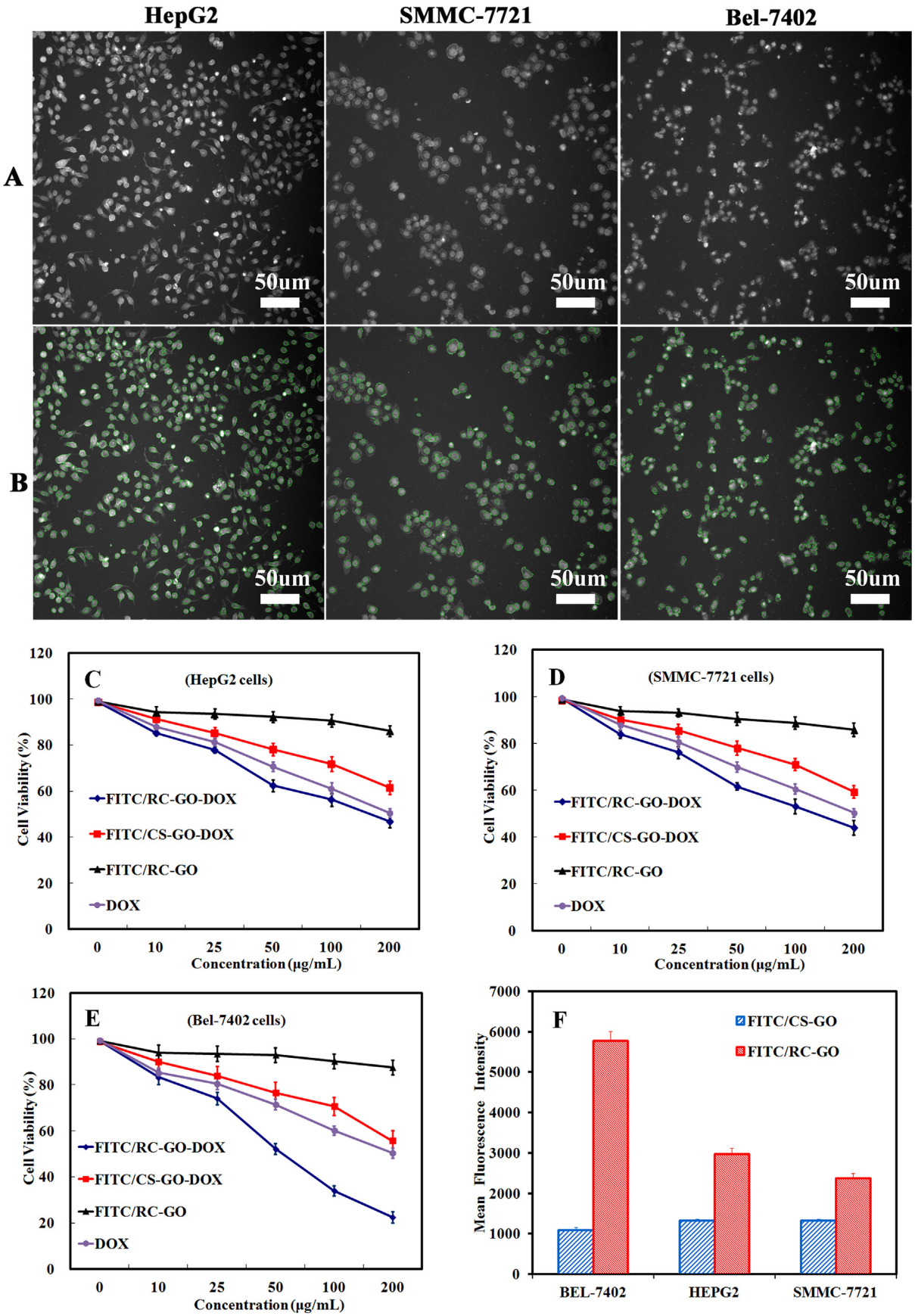


**Fig. 8.** High-content screening image analysis. (A and B) Images in rows A and B show the same field of hepatoma cells post 48-h incubation before and after application of the High Content Analysis Reader. (C–E) Relative cell viability of three hepatoma cell lines after treatment with RC–GO–DOX, CS–GO–DOX, RC–GO and DOX for 48 h. Cytotoxicity was evaluated by CCK-8 assay. The values given are mean ± SD and $n = 3$. (F) Mean fluorescence intensity of different samples determined in HepG2 cells, SMMC-7721 cells and Bel-7402 cells.

### 3.5. The release mechanism of DOX

Based on the structure of DOX, GO and cRGD-modified chitosan, there can be a hydrophobic interaction (including π–π stacking), hydrogen bonding and an electrostatic interaction among these three molecules, all of which are pH-dependent.

Under neutral conditions (pH 7.4), the —COOH and —OH groups on GO may interact with the —$NH_2$ and —OH groups on DOX, forming hydrogen bonds. When pH decreases (pH 5.5), the $NH_2$ groups of DOX become protonated ($NH_3^+$). The protonate may result in the partial dissociation of hydrogen bonds, and the amount of DOX released from GO is greater. The hydrogen-bonding interaction may also be weakened because of the hydrogen ions in solution, which would compete with the hydrogen bond-forming groups. In addition, the hydrogen bond interaction is weakened because of the hydrogen ions in solution, which compete with the hydrogen bond-forming groups.

An electrostatic interaction may play a role in the release process. The electrostatic interaction between GO and cRGD-modified chitosan would be weakened at a low pH (pH 5.5), because GO was less negatively charged under acid conditions [55], which may promote the release of DOX. The polymer cRGD-modified chitosan also degrades to an even greater extent at pH 5.5.

In summary, the hydrophobic force (including π–π stacking), hydrogen bonding and electrostatic interaction may affect the drug release of DOX at different pH values. In view of the high loading capacity and pH-responsive drug release of the polymer with regard to DOX, it appears to be a favorable material for drug delivery applications and controlled drug release.

### 3.6. Cell targeting ability of RC–GO–DOX

To visualize the cellular uptake of FITC/RC–GO and FITC/CS–GO, the green fluorescence emitted by FITC was captured by LCFM after the polymers were incubated with HepG2 cells and SMMC-7721 cells, which have a low expression of integrin $\alpha_v\beta_3$, and Bel-7402 cells, which over-express integrin $\alpha_v\beta_3$. In Fig. 7, the weak green fluorescence of FITC in Bel-7402 cells indicates that a low amount of FITC/CS–GO had entered tumor cells. Similarly, the amount of FITC/CS–GO that entered the HepG2 cells and SMMC-7721 cells was so low that there was no significant difference between the fluorescence intensity of the different groups of cells. By contrast, FITC/RC–GO in Bel-7402 tumor cells showed obvious green fluorescence. The mean fluorescence intensity of the three cell lines incubated with different samples was imaged and analyzed using the high-content screening (HCS). From the HCS results in Fig. 8A, B, and F, it was found that the mean fluorescence intensity of tumor cells incubated with cRGD-modified polymers was always much higher than that with normal polymers without modification.

### 3.7. Cell viability

The CCK-8 test was used to evaluate the effects of the polymers on living cell metabolic activity. As shown in Fig. 8C–E, no obvious cytotoxicity (>80% cell viability) was observed for the FITC/RC–GO polymers without DOX loading, even at concentrations as high as 200 μg/mL for the three kinds of cells. This indicates the low cytotoxicity and favorable biocompatibility of FITC/RC–GO polymers, although both types of DOX-loaded polymers inhibit the growth of hepatocarcinoma cells in vitro. The observed results show that FITC/RC–GO–DOX polymers exhibit higher concentration-dependent cytotoxicity (0–200 μg/mL) with the three kinds of cells than FITC/CS–GO–DOX polymers. This indicates that the potential advantage of using FITC/RC–GO–DOX polymers as a drug carrier is their ability to produce targeted delivery for the selective destruction of hepatoma cells. It is worth pointing out that FITC/RC–GO polymers do not significantly reduce cell viability, indicating their good biocompatibility, which is due to the excellent intrinsic biocompatibility of chitosan and GO. These results suggest that FITC/RC–GO–DOX polymers as a drug delivery system can be expected to have a great potential for selectively enhancing the cytotoxic effect of DOX on hepatoma carcinoma cells.

## 4. Conclusion

In this investigation, we successfully produced and characterized an innovative multifunctional drug delivery system with the ability to target hepatocarcinoma cells, produce controlled drug release, in a pH-responsive manner, and with efficient loading. GO has large specific surface in this system, resulting in a higher loading capacity (1.00 mg/mg). The drug-loaded polymer system displays a pH-responsive behavior, which may offer excellent stability under physiological conditions but produce release at a reduced pH (cancerous tissue environment). A higher pH leads to a weaker hydrophobic interaction and hydrogen bonding, resulting in a greater release rate. The cellular uptake of RC–GO–DOX polymers was significantly increased in hepatoma cells (especially for Bel-7402 cells, the integrins-overexpressed cells), compared with the polymers without cRGD peptides modification. Drug-loaded polymers exhibit greater cytotoxic effects on hepatoma cells than other types of polymers. Based on these favorable results, we can conclude that this new system may be used in biomedical applications, and may improve the efficacy of HCC therapy. Further work will be needed to investigate the details of the inhibition of tumor growth by the polymers in order to gain more information about how the delivery system works, and also to extend this application to several other small molecular weight chemotherapeutic agents of interest.

## Acknowledgements

This research was supported by the Scientific Research Foundation of Fujian Provincial Department of Public Health (No. 2012-2-110) and the Scientific Research Foundation of Xiamen Medical College (No. K2010-2).

## References

[1] A. Villanueva, J.M. Llovet, Gastroenterology 140 (2011) 1410.
[2] L.E. van Vlerken, Z. Duan, M.V. Seiden, M.M. Amiji, Cancer Res. 67 (2007) 4843.
[3] L. Li, H. Wang, Z.Y. Ong, K. Xu, P.L.R. Ee, S. Zheng, J.L. Hedrick, Y.-Y. Yang, Nano Today 5 (2010) 296.
[4] L. Fiume, M. Baglioni, L. Bolondi, C. Farina, G. Di Stefano, Drug Discov. Today 13 (2008) 1002.
[5] S. Prakash, M. Malhotra, W. Shao, C. Tomaro-Duchesneau, S. Abbasi, Adv. Drug Deliv. Rev. 63 (2011) 1340.
[6] R. Singh, J.W. Lillard, Exp. Mol. Pathol. 86 (2009) 215.
[7] F. Danhier, O. Feron, V. Préat, J. Control. Release 148 (2010) 135.
[8] F. Marcucci, F. Lefoulon, Drug Discov. Today 9 (2004) 219.
[9] D.C. Drummond, O. Meyer, K.L. Hong, D.B. Kirpotin, D. Papahadjopoulos, Pharmacol. Rev. 51 (1999) 691.
[10] C. Maderuelo, A. Zarzuelo, J.M. Lanao, J. Control. Release 154 (2011) 2.
[11] S.R. Saks, L.B. Gardner, J. Control. Release 48 (1997) 237.
[12] M. Dash, F. Chiellini, R.M. Ottenbrite, E. Chiellini, Progress Polym. Sci. 36 (2011) 981.
[13] L. Zhou, W. Wang, J. Tang, J.-H. Zhou, H.-J. Jiang, J. Shen, Chem.: Eur. J. 17 (2011) 12084.
[14] Q. Huamin, F. Lulu, X. Li, L. Li, S. Min, L. Chuannan, Carbohydr. Polym. 92 (2013) 394.
[15] V. Singh, D. Joung, L. Zhai, S. Das, S.I. Khondaker, S. Seal, Progress Mater. Sci. 56 (2011) 1178.
[16] T. Kuila, S. Bose, P. Khanra, A.K. Mishra, N.H. Kim, J.H. Lee, Biosens. Bioelectron. 26 (2011) 4637.
[17] S. Alwarappan, A. Erdem, C. Liu, C.Z. Li, J. Phys. Chem. C 113 (2009) 8853.
[18] S. Alwarappan, C. Liu, A. Kumar, C.Z. Li, J. Phys. Chem. C 114 (2010) 12920.
[19] Z. Tang, H. Wu, J.R. Cort, G.W. Buchko, Y. Zhang, Y. Shao, I.A. Aksay, J. Liu, Y. Lin, Small 6 (2010) 1205.
[20] F. Li, Y. Huang, Q. Yang, Z. Zhong, D. Li, L. Wang, S. Song, C. Fan, Nanoscale 2 (2010) 1021.

[21] S. He, B. Song, D. Li, C. Zhu, W. Qi, Y. Wen, L. Wang, S. Song, H. Fang, C. Fan, Adv. Funct. Mater. 20 (2010) 453.
[22] C.-H. Lu, H.-H. Yang, C.-L. Zhu, X. Chen, G.-N. Chen, Angew. Chem. Int. Ed. 48 (2009) 4785.
[23] W. Qin, X. Li, W.-W. Bian, X.-J. Fan, J.-Y. Qi, Biomaterials 31 (2010) 1007.
[24] W.B. Hu, C. Peng, W.J. Luo, M. Lv, X.M. Li, D. Li, Q. Huang, C.H. Fan, ACS Nano 4 (2010) 4317.
[25] V.K. Rana, M.-C. Choi, J.-Y. Kong, G.Y. Kim, M.J. Kim, S.-H. Kim, S. Mishra, R.P. Singh, C.-S. Ha, Macromol. Mater. Eng. 296 (2011) 131.
[26] D. Depan, J. Shah, R.D.K. Misra, Mater. Sci. Eng. C 31 (2011) 1305.
[27] Z. Liu, J.T. Robinson, X.M. Sun, H.J. Dai, J. Am. Chem. Soc. 130 (2008) 10876.
[28] L. Zhang, J. Xia, Q. Zhao, L. Liu, Z. Zhang, Small 6 (2010) 537.
[29] Z. Gu, T.T. Dang, M.L. Ma, B.C. Tang, H. Cheng, S. Jiang, Y.Z. Dong, Y.L. Zhang, D.G. Anderson, ACS Nano 7 (2013) 6758.
[30] S.J. Lee, M.S. Huh, S.Y. Lee, S. Min, S. Lee, H. Koo, J.U. Chu, K.E. Lee, H. Jeon, Y. Choi, K. Choi, Y. Byun, S.Y. Jeong, K. Park, K. Kim, I.C. Kwon, Angew. Chem. Int. Ed. 51 (2012) 7203.
[31] C. Duan, J. Gao, D. Zhang, L. Jia, Y. Liu, D. Zheng, G. Liu, X. Tian, F. Wang, Q. Zhang, Biomacromolecules 12 (2011) 4335.
[32] P. Yousefpour, F. Atyabi, E. Vasheghani-Farahani, A.A.M. Movahedi, R. Dinarvand, Int. J. Nanomed. 6 (2011) 1977.
[33] R.S. Tigli, M. Gumusderelioglu, Int. J. Biol. Macromol. 43 (2008) 121.
[34] C.Y. Zhan, B. Gu, C. Xie, J. Li, Y. Liu, W.Y. Lu, J. Control. Release 143 (2010) 136.
[35] X.B. Xiong, A. Mahmud, H. Uludag, A. Lavasanifar, Biomacromolecules 8 (2007) 874.
[36] H.Y. Tian, L. Lin, J. Chen, X.S. Chen, T.G. Park, A. Maruyama, J. Control. Release 155 (2011) 47.
[37] J. Kim, H.Y. Nam, T.I. Kim, P.H. Kim, J. Ryu, C.O. Yun, S.W. Kim, Biomaterials 32 (2011) 5158.
[38] Y. Vachutinsky, M. Oba, K. Miyata, S. Hiki, M.R. Kano, N. Nishiyama, H. Koyama, K. Miyazono, K. Kataoka, J. Control. Release 149 (2011) 51.
[39] D.B. Pike, H. Ghandehari, Adv. Drug Deliv. Rev. 62 (2010) 167.
[40] C.C. Kumar, Curr. Drug Targets 4 (2003) 123.
[41] Y.Q. Ge, Y. Zhang, S.Y. He, F. Nie, G.J. Teng, N. Gu, Nanoscale Res. Lett. 4 (2009) 287.
[42] L. Zhou, H. Jiang, S. Wei, X. Ge, J. Zhou, J. Shen, Carbon 50 (2012) 5594.
[43] X.Y. Yang, X.Y. Zhang, Z.F. Liu, Y.F. Ma, Y. Huang, Y. Chen, J. Phys. Chem. C 112 (2008) 17554.
[44] H.D. Han, L.S. Mangala, J.W. Lee, M.M.K. Shahzad, H.S. Kim, D.Y. Shen, E.J. Nam, E.M. Mora, R.L. Stone, C.H. Lu, S.J. Lee, J.W. Roh, A.M. Nick, G. Lopez-Berestein, A.K. Sood, Clin. Cancer Res. 16 (2010) 3910.
[45] F.P. OuYang, B. Huang, Z.Y. Li, J. Xiao, H.Y. Wang, H. Xu, J. Phys. Chem. C 112 (2008) 12003.
[46] C. Velasco-Santos, A.L. Martinez-Hernandez, V.M. Castano, J. Phys. Chem. B 108 (2004) 18866.
[47] D.M. Guldi, M. Marcaccio, D. Paolucci, F. Paolucci, N. Tagmatarchis, D. Tasis, E. Vázquez, M. Prato, Angew. Chem. Int. Ed. 42 (2003) 4206.
[48] H. Murakami, T. Nomura, N. Nakashima, Chem. Phys. Lett. 378 (2003) 481.
[49] A. Lerf, H.Y. He, M. Forster, J. Klinowski, J. Phys. Chem. B 102 (1998) 4477.
[50] J. Liu, S. Guo, L. Han, W. Ren, Y. Liu, E. Wang, Talanta 101 (2012) 151.
[51] D. Han, L. Yan, W. Chen, W. Li, Carbohydr. Polym. 83 (2011) 653.
[52] L.L. Ren, T.X. Liu, J.A. Guo, S.Z. Guo, X.Y. Wang, W.Z. Wang, Nanotechnology 21 (2010).
[53] W. Ren, Y.X. Fang, E.K. Wang, ACS Nano 5 (2011) 6425.
[54] X. Zhang, L. Meng, Q. Lu, Z. Fei, P.J. Dyson, Biomaterials 30 (2009) 6041.
[55] R. Zhang, M. Hummelgård, G. Lv, H. Olin, Carbon 49 (2011) 1126.